Theta oscillations and sensorimotor performance

Leslie M. Kay*

Department of Psychology, Institute for Mind and Biology, University of Chicago, 940 East 57th Street, Chicago, IL 60637

Edited by Nancy J. Kopell, Boston University, Boston, MA, and approved January 28, 2005 (received for review October 25, 2004)

Performance and cognitive effort in humans have recently been related to amplitude and multisite coherence of alpha (7–12 Hz) and theta (4–7 Hz) band electroencephalogram oscillations. I examined this phenomenon in rats by using theta band oscillations of the local field potential to signify sniffing as a sensorimotor process. Olfactory bulb (OB) theta oscillations are coherent with those in the dorsal hippocampus (HPC) during odor sniffing in a two-odor olfactory discrimination task. Coherence is restricted to the high-frequency theta band (6–12 Hz) associated with directed sniffing in the OB and type 1 theta in the HPC. Coherence and performance fluctuate on a time scale of several minutes. Coherence magnitude is positively correlated with performance in the two-odor condition but not in extended runs of single odor conditional-stimulus-positive trials. Simultaneous with enhanced OB–HPC theta band coherence during odor sniffing is a significant decrease in lateral entorhinal cortex (EC)–HPC and OB–EC coherence, suggesting that linkage of the olfactory and hippocampal theta rhythms is not through the synaptic relay from OB to HPC in the lateral EC. OB–HPC coupling at the sniffing frequency is proposed as a mechanism underlying olfactory sensorimotor effort as a cognitive process.

hippocampus | olfactory bulb | sniffing | behavior | odor discrimination

Within a given day, performance measures can change, depending on multiple factors. The neural mechanisms that underlie these performance fluctuations in motor and cognitive tasks remain unexplained, with some studies focusing on theta (4–7 Hz in humans and 4–12 Hz in rats) and alpha (7–12 Hz) oscillations as indicators of cognitive effort associated with performance in difficult tasks (1–6).

The mammalian hippocampus (HPC) and olfactory bulb (OB) are distinguished by high-amplitude theta oscillations of the local field potential. Hippocampal theta rhythm (4–12 Hz in rats) has been shown to accompany locomotion and cognitive processing, and two theta subbands have been described. High-frequency theta (type 1: 6–12 Hz, atropine-resistant) is linked to locomotion, and low-frequency theta (type 2: 4–6 Hz, atropine-sensitive) is seen during immobile states, sensory stimulation, and in urethane-anesthetized animals (7). In the OB, 2- to 12-Hz oscillations have been shown to follow the respiratory cycle with some deviations, and these oscillations are called "theta" principally because they occupy a highly overlapping frequency band with hippocampal theta oscillations (8–13).

HPC theta oscillations and sniffing have been related to performance and learning in previous studies. Theta oscillatory firing of single interneurons in the HPC has been shown to be related to performance in a cognitively demanding olfactory identification task (14). Hippocampal theta oscillations have also been shown to be coherent with sniffing during the initial stages of odor contingency reversal learning (15) and with OB theta oscillations intermittently during exploratory behavior (16).

In this study, I examine the role of theta oscillations in olfactory performance by relating hippocampal theta oscillations recorded from the dorsal HPC at the hilus of the dentate gyrus (DG) to those of similar frequency in the OB during an olfactory identification and response task. The changes in interaction of these two rhythms are tracked within trials and during the course of experimental sessions. A significant positive correlation is shown between OB–HPC theta rhythm coherence (during odor sniffing) and task performance, both of which fluctuate on the order of 5–10 min. This coherence may represent a mechanism whereby sensory, motor, and cognitive structures participate cooperatively in sensory discrimination.

Methods

Experiments. Four adult male Sprague–Dawley rats were implanted with electrodes under pentobarbital anesthesia by using stereotaxic coordinates as a guide and lateral olfactory tract stimulation for precise positioning. Stainless steel electrodes were placed in the lateral olfactory tract, OB, anterior piriform cortex (aPC), lateral entorhinal cortex (EC), and the dorsal HPC at the hilus of the DG. After recovery, all rats were dieted to 85% of their ad libitum weight and maintained on a restricted diet throughout training and testing. All animal procedures were done in accordance with the Association for Assessment and Accreditation of Laboratory Animal Care guidelines under approved animal use protocols.

The four rats were trained to respond to a conditional stimulus $(CS)^+$ odor (almond or orange extract) by pressing a lever in one end of a modified home cage. The reward (one drop of 10% sucrose solution) was delivered from a drinking tube inside the odor port, and the reward lever was situated just below the odor port. Three-second odor pulses were delivered on a fixed intertrial interval (12 s), and the animals were required to refrain from pressing the lever for 1 s in each trial, beginning 0.5 s before the onset of the odor pulse ("no press" in Fig. 1). The penalty for pressing during the no press period was disabling of the reward for that trial. There was no penalty for pressing the lever before the no press period or at any time during the CS^- trials, although the rats pressed only rarely after odor presentation in these trials. Every 12 s, the odor was either the CS^+ or one of two CS^- unrewarded odors (the other in the pair of orange or almond extract or plain air) injected into the constant airstream. The CS^+ and CS^- trials were pseudorandomly interleaved, with $\approx$50% CS^+ and 50% CS^- trials. There were 31 1.5- to 2.5-h operant test sessions (100–250 trials) across the four animals. Four sessions had insufficient data for longitudinal analysis.

Signals were recorded differentially with reference to a skull screw and digitized at 2 kHz (analog filters 1–300 Hz). Six seconds were recorded for each trial, 3.5 s before the onset of the odor and 2.5 s after the onset of the 3.0-s odor pulse. A unity gain preamplifier headstage (NB Labs, Denison, TX) was used for signal conditioning.

Electrode placements were verified during the many months' duration of the implant by electrical stimulation of the implanted lateral olfactory tract electrode, with the same protocol as that used during surgery (see *Supporting Methods*, which is published as supporting information on the PNAS web site). In particular, the HPC electrodes were verified in this manner so that the evoked response indicated that the electrode was in or near the DG at the hilus. At the end of the experiments, the rats were

This paper was submitted directly (Track II) to the PNAS office.

Abbreviations: OB, olfactory bulb; aPC, anterior piriform cortex; EC, entorhinal cortex; DG, dentate gyrus; HPC, hippocampus; CS, conditional stimulus.

*E-mail: lkay@uchicago.edu.

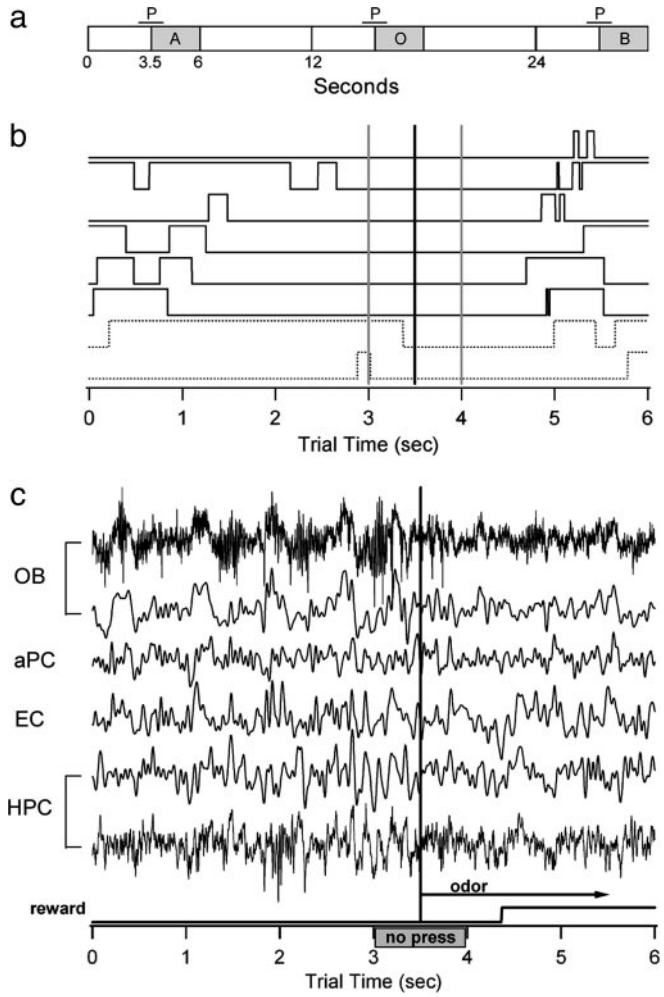

Fig. 1. Trial design and sample data. (*a*) Schematic of the fixed timing of trials showing successive CS^+ odor (A), plain air (O) and CS^- odor (B) trials. P, no press period. (*b*) Examples of lever pressing performance showing that the rats can anticipate the arrival of the odor stimulus. Dark traces are correct CS^+ trials, and dashed traces are incorrect CS^+ trials. Vertical gray lines surround the no press period, and the vertical black line indicates the odor onset time. (*c*) Simultaneously recorded data from the four brain areas. Theta band data are 1–20 Hz. Raw data (1–300 Hz) are shown for the OB and HPC. Note the change in character of the theta rhythm beginning with the onset of the no press period and again with the odor onset, transitioning in the OB to low amplitude and high frequency, which is consistent with the transition to sniffing.

euthanized with an overdose of sodium pentobarbital. Electrolytic lesions were made to mark the electrode sites using the Prussian Blue reaction, and the brain was fixed by means of transcardial perfusion. The brains were removed, sectioned, and examined under a dissection microscope to verify electrode locations. It was not possible to verify the positions of recording electrodes for each session, and it is common for electrode placements to drift over time. Thus, the final electrode locations were estimates of the positions for recordings taken over 3–4 months.

Data were digitally filtered (low pass at 20 Hz; IGOR FILTER DESIGN LABORATORY, WaveMetrics, Lake Oswego, OR), and all further analyses were done on the filtered data. Power spectra were estimated by using a Hanning taper from specified 1,024-ms time windows across 10–25 trials of the same odor and contingency, with the number of trials determined by the specific analysis (see below). For dynamic spectra, this window was stepped through the behavioral trial (0.25-s steps) to create an averaged matrix of power spectral density or coherence that spanned the theta frequency band and the 6-s trial time.

Analysis. Coherence was estimated from the averaged power spectra of 1,024-ms time windows from 10–25 trials [depending on whether the global (25 trials) or moving (10–15 trials) average was used] from individual channels and from the cross-spectral estimates across pairs of channels, as described in ref. 17.

Performance was calculated as the percentage of correct responses to all trials in blocks spanning 10–15 CS^+ trials, stepped by one trial so that each trial had a percentage associated with it that referred to the previous ≈20–30 trials, including interleaved CS^- trials, and spanning ≈4–8 min. Correct responses are considered to be: (*i*) CS^+ trials in which the lever press was timed appropriately to deliver the reward, and (*ii*) CS^- trials in which no lever press was performed from 3.0–6.0 s in a trial. Incorrect trials could include early presses for CS^+, remaining on the lever for the entire trial, not pressing the lever for the CS^+, or pressing the lever during any part of the odor period for CS^- trials ($12 \pm 7\%$ of CS^- trials in a session). Careful notes were made on each trial in which the animal did not approach the odor port at the appropriate time. These trials were excluded and did not account for >5% of the total trials. Data were then sorted by stimulus type, and CS^+ trials were used for longitudinal analysis because of the explicit requirement for a behavioral response and the larger number of trials with a single odor condition.

Longitudinal power and coherence spectra were estimated on blocks of 10–15 CS^+ trials, stepped by 1–10 trials, as described in *Results*. The number of CS^+ trials per block depended on the data available. In sessions of ≈200 trials, blocks of 15 trials were used, whereas, in sessions with ≈100 trials, blocks of 10 trials were used. Blocks were stepped by one trial to provide more data for the measures, but each data set was also tested with larger steps, corresponding to half-overlapping blocks of trials (five to eight trial steps, depending on the size of the trial block). Coherence and correlation estimates were compared with identical analyses on the same data sets with channels shuffled across trials.

Results

The focus of this report is on theta band activity, and of particular importance is how theta oscillations relate to changes in stereotyped behavior over the course of a trial and to fluctuations in task performance over the course of a recording session. To this end, I characterize the frequency and coherence of theta activity in the olfactory and hippocampal systems as they relate to behavior within a trial and over blocks of trials. Thus, the data are analyzed in five successively more focused steps to characterize behavior, theta frequency changes within trials, theta band coherence changes within trials, fluctuations of theta coherence magnitude during odor sniffing across trial blocks, and correlation of OB–HPC coherence magnitude fluctuation with task performance changes.

Behavior. The odor stimulus (3 s) was injected into the continuous airstream in the odor port, beginning at the 3.5-s mark in each trial, and the only cue for the onset of this period was the fixed intertrial interval (Fig. 1*a*). Therefore, it is evident that the animals learned the timing of the odor very well because of the onset of fast sniffing in anticipation of the odor and by trials in which they pressed the lever during the time preceding the no press period but refrained from pressing the lever during the no press period (Fig. 1 *b* and *c*). Local field potential data were collected from the OB, aPC, EC, and HPC while the rats performed the odor discrimination task. In all, 31 operant test sessions over four rats were analyzed.

Odor discrimination was not difficult for the rats, because

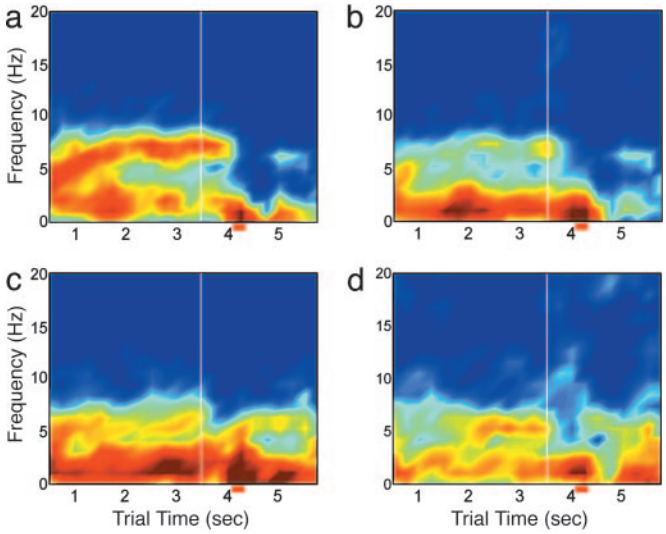

Fig. 2. Dynamic power spectra show changes over the behavioral epochs. Averaged power spectra are shown for the four recording sites across a set of 25 nonconsecutive CS^+ trials chosen for similarity in response time. Spectra are estimated for each 1,024-ms time window, stepped by 250 ms. Odor onset is indicated by the vertical white line at 3.5 s, and the average response time ± standard deviation is shown below each matrix (red horizontal bar). Color scale indicates log dimensionless power and is constant for the four plots. (*a*) OB frequencies occupy all parts of the theta band, with 7–10 Hz predominating during the sniffing period. (*b*) aPC theta is similar to that in the OB. (*c*) EC theta oscillations cover the lower end of the theta band, from 4 to 7 Hz, rarely showing peaks in the higher portion of the band. (*d*) HPC theta occupies two bands corresponding to the definitions of type 1 (7–12 Hz) and type 2 (4–6 Hz) theta. Very low-frequency power in all spectra is due to the 1/f nature of the power spectra in most cortical areas. The data have been log-transformed to attenuate this effect.

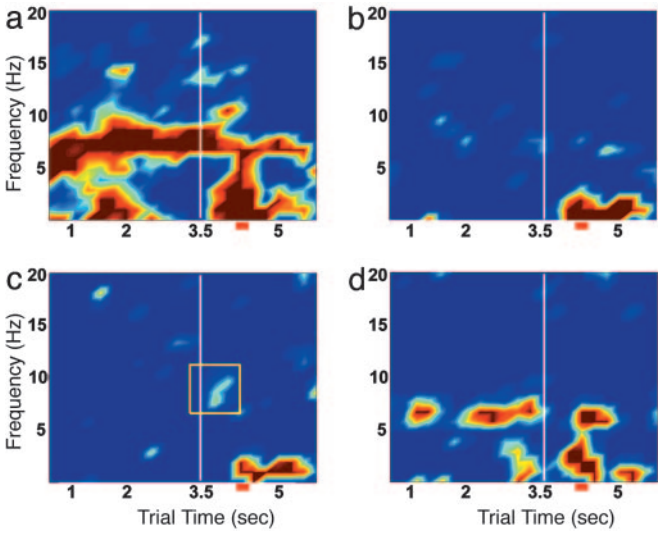

Fig. 3. Dynamic coherence spectra show differences in functional connectivity across behavioral epochs. Pairwise coherence spectra are shown for the same data as in Fig. 2. (*a*) OB–aPC. (*b*) OB–EC. (*c*) OB–HPC. (d) EC–HPC. Note significant coherence after odor onset for the OB–HPC pair and the interruption of coherence for the OB–EC and EC–HPC pairs. The yellow square in *c* marks the time and frequency domain in which coherence occurs during odor sniffing. This segment of data is used for the coherence statistics represented in Figs. 5 and 11. OB–EC coherence can be strong or weak in the prestimulus period. Examples of strong OB–EC coherence, also interrupted with the onset of odor sniffing, are shown in Fig. 7. Scale is constant for the four plots, with dark blue representing the threshold for significance as compared with shuffled data. The overall performance for this experiment was 68.3%. (More OB–HPC coherence examples are shown in Fig. 8.)

initial CS^+/CS^- training was accomplished in one session after they learned to bar press to an odor to receive a reward. The timing of the task was the difficult feature, because it required the animals to anticipate an odor stimulus solely from the fixed intertrial interval of 12 s. All rats learned the task in unrecorded training sessions to criterion (>65% correct; 7–21 days total per rat). After training, each individual's performance varied across sessions (45% to ≈100% correct for complete sessions of 100–250 trials). Variations in performance were also seen within sessions, as is discussed below. Some sessions contained long stretches of CS^+ trials only (20 or more trials) at the beginning or end of the session to examine changes related to task type. Theta oscillations indicative of respiratory changes in the OB often change in amplitude and frequency before or with the onset of the "no press" period before the onset of the odor stimulus (Fig. 1*c*). Locomotor activity was minimal, particularly as the rats gained more experience and sat in front of the odor port almost continuously, rarely exploring the test chamber. Thus, the HPC theta rhythm differs from that seen in rodents performing exploratory behavior.

Theta Frequency Patterns. Respiration is represented in the OB by the theta rhythm (8, 10, 18), and this rhythm was used as an internal estimate of sniffing rate as was done previously (12, 17). Power spectra were determined for 1,024-ms time windows stepped by 250 ms to create a dynamic averaged power spectrum through the trial time, averaged across a set of 25 trials chosen for similar response times (Fig. 2). Peak theta rhythms in the OB advance from as low as 3–5 Hz at the beginning of trials to 6–10 Hz during the odor identification period (Fig. 2*a*). A similar pattern can be seen in the aPC, although at much lower power (Fig. 2*b*). The EC often maintains a peak theta rhythm in the 4–6 Hz band typical of type 2 hippocampal theta rhythm throughout the entire trial (Fig. 2*c*). The HPC maintains the slower theta rhythm and shows an additional higher frequency theta rhythm (7–12 Hz) during the odor identification period (Fig. 2*d*). OB theta frequencies can occupy low or high frequencies and any of the frequencies in between, depending on respiration rates (Fig. 2*a*). In contrast, HPC theta frequencies, as measured at or near the hilus of the DG occur in what appear to be two separate bands at ≈3–6 and 7–13 Hz, without a smooth transition in frequency from one to the other (Fig. 2*d*).

Dynamic Theta Coherence Patterns. Coherence analysis allows examination of signals that are cooperative between brain areas. Dynamic coherence shows the change of this cooperativity over the course of a behavioral trial. Sample coherence patterns from four pairs of the four brain areas across the task are shown (Fig. 3; the two additional pairs, aPC–EC and aPC–HPC, are shown in Fig. 6, which is published as supporting information on the PNAS web site). The OB and aPC show high coherence at the sniffing frequency (Fig. 3*a*). The OB and EC often show coherence in the theta band close to that of the EC theta rhythm, although the coherence is faint in this example (Fig. 3*b*; see Fig. 7, which is published as supporting information on the PNAS web site, for other examples), and this coherence is interrupted with the onset of the odor stimulus. The OB and HPC show significant coherence reliably during the sniffing period only (Fig. 3*c* and Fig. 8, which is published as supporting information on the PNAS web site), although this coherence can be found in parts of the prestimulus region as well (Figs. 7*d* and 8*c*). When OB–HPC coherence is measured from large or noncontiguous trial blocks, it is sometimes weak, as in Fig. 3*c*, or even insignificant, whereas, in others, it can be quite strong (Figs. 7 *a* and

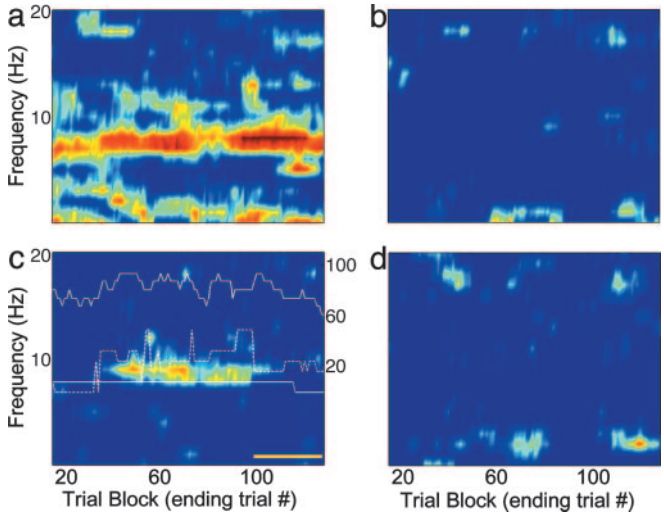

Fig. 4. Functional connectivity may vary during the course of a test session. Longitudinal coherence from the odor sniffing period (3.25–4.25 s) is shown for four electrode pairs. Each horizontal point is estimated from 15 consecutive CS^+ trials ending with the trial number on the horizontal axis. Values of lighter hue than the dark blue background are significantly above the average coherence values for shuffled data. (*a*) OB–aPC. The dominant coherence band matches the sniffing frequency estimated from the OB theta frequency during odor sampling (7.8 Hz). (*b*) OB–EC. There is virtually no coherence between these two areas in the theta band during odor sniffing. (*c*) OB–HPC. The OB (lower solid white trace) and HPC (dashed white line) peak high theta frequencies (7–13 Hz) are shown overlaid, as are performance statistics (upper solid white trace; right axis). Note the long stretch of trials in which significant coherence is seen in the band spanned by the OB and HPC peak theta frequencies and that this corresponds to an extended period of higher performance values. The region indicated by the yellow line is a run of CS^+ trials delivered at the end of the session. (*d*) EC–HPC. There is no coherence in this band during odor sniffing; although, during other periods, the coherence is high (see Fig. 3*d*).

d and 8 *b* and *d*). In the next section, this variability in the coherence measure is examined in more detail. The EC and HPC show a coherent band primarily in the 4- to 7-Hz range that is interrupted with the onset of odor sniffing, with a significant decrease in coherence relative to preodor periods of 24.2 ± 4.9% (paired *t* test; $P < 10^{-6}$) (Figs. 3*d* and 7 *c* and *e*).

Significant OB–HPC coherence did not depend on positive association or the operant nature of the task, because coherence was present during odor sniffing in operant CS^- trials and in sessions in which rats were conditioned in a classical paradigm to associate delivery of a reward after one of two odors (Fig. 9, which is published as supporting information on the PNAS web site).

Within-Session Variation in OB–HPC Theta Coherence. Although interesting dynamics were seen for all pairs of structures, I concentrate here on OB–HPC within-session coherence fluctuations. There was significant variability in the strength of OB–HPC coherence during the sniffing period within sessions. The analysis in this section addresses coherence pattern variations on a time scale of a few minutes, shorter than the 1.5–2.5 h of the entire session.

In some subsets of consecutive trials within each session the OB–HPC coherence was insignificant, whereas in others it was very high. To describe these changes in coherence, a longitudinal analysis was applied to the sniffing period (3.25–4.25 s) in consecutive trial blocks (Fig. 4). This window begins just before odor onset and ends just after the no press period. With a taper applied to the window, the central portion is emphasized so that the period of analysis is primarily the 0.5 s of fast odor sniffing at the onset of the odor pulse. The OB and aPC show a strong and persistent coherence during odor sniffing throughout the experiment (Fig. 4*a*). The OB–EC and EC–HPC (Fig. 4 *b* and *d*) longitudinal profiles show a marked absence of coherence at the sniffing frequency during this same period, as seen in the dynamic coherence profiles (Figs. 3 *b* and *d* and 7 *b* and *d*). The OB and HPC show an extended period of strong coherence in high frequency theta flanked by periods in which coherence drops below significant levels in this case (Fig. 4*c*). In other sessions, the coherent periods come and go, with a discontinuous pattern (see Fig. 10, which is published as supporting information on the PNAS web site).

Correlated Fluctuations OB–HPC Coherence Magnitude and Performance. To more closely examine a behavioral explanation of OB–HPC coherence intermittency, performance measures (percent correct, as described in *Methods*) were calculated for each block of trials spanned by 15 CS^+ trials, and then the CS^+ trials were isolated for analysis. The performance level for each block was linked with the CS^+ trial ending the block, so that for each trial there was an associated measure of how well the animal performed on all of the trials (CS^+, CS^-, and no odor trials) spanned by the current CS^+ trial together with the previous 14 CS^+ trials.

Correlation between OB–HPC coherence in CS^+ trials and performance was consistently significant and positive in the two-odor discrimination (Fig. 5), and this measure accounted for the variation in coherence seen within individual sessions. In only one of 27 sessions across four animals was the correlation insignificant (for more examples, see Fig. 10 and Fig. 11, which is published as supporting information on the PNAS web site). In 4 of the 31 sessions, there were not enough artifact-free trials to perform the longitudinal analysis. The positive correlation between coherence and performance was consistent only in the two-odor task. In several sessions, rats were given extended runs of single-odor CS^+ trials (30–50 trials), and in these cases OB–HPC coherence was also observed, but it had either negative or insignificant correlation with performance (four and three sessions, respectively) (Fig. 5 *a* and *d*). Coherence magnitude in prestimulus periods of the trials did not show a consistent relationship with performance across sessions or animals ($P > 0.05$).

Discussion

Previous studies regarding the involvement of the HPC in odor-guided behavior have focused primarily on associative learning (19–21), although some have shown hippocampal involvement in well learned behaviors (14, 22). Studies of HPC theta rhythm focus primarily on recordings within one area of the HPC or within multiple subfields of the EC and HPC. Looking beyond the hippocampal formation can provide insight into processing modes that are correlated with behavioral states. The data reported here show significant involvement of the HPC in performance of a well learned two-odor operant olfactory task. This involvement is characterized by OB–HPC theta band coherence at the sniffing frequency correlated strongly with performance (Fig. 5).

Significant positive correlation between type 1 theta band OB–HPC coherence magnitude and performance was restricted to experiments and parts of experiments where two odors and their opposite contingencies were present (Fig. 5). This finding is consistent with the necessity for an intact HPC and parahippocampal area for odor–odor associations but not single-odor habituation (23, 24). The positive correlation seen here is opposite in sign to the sniffing and HPC theta coherence observed during contingency reversal learning in an earlier study (15). In that study, theta oscillations were coherent with sniffing during early odor contingency reversal learning, with coherence

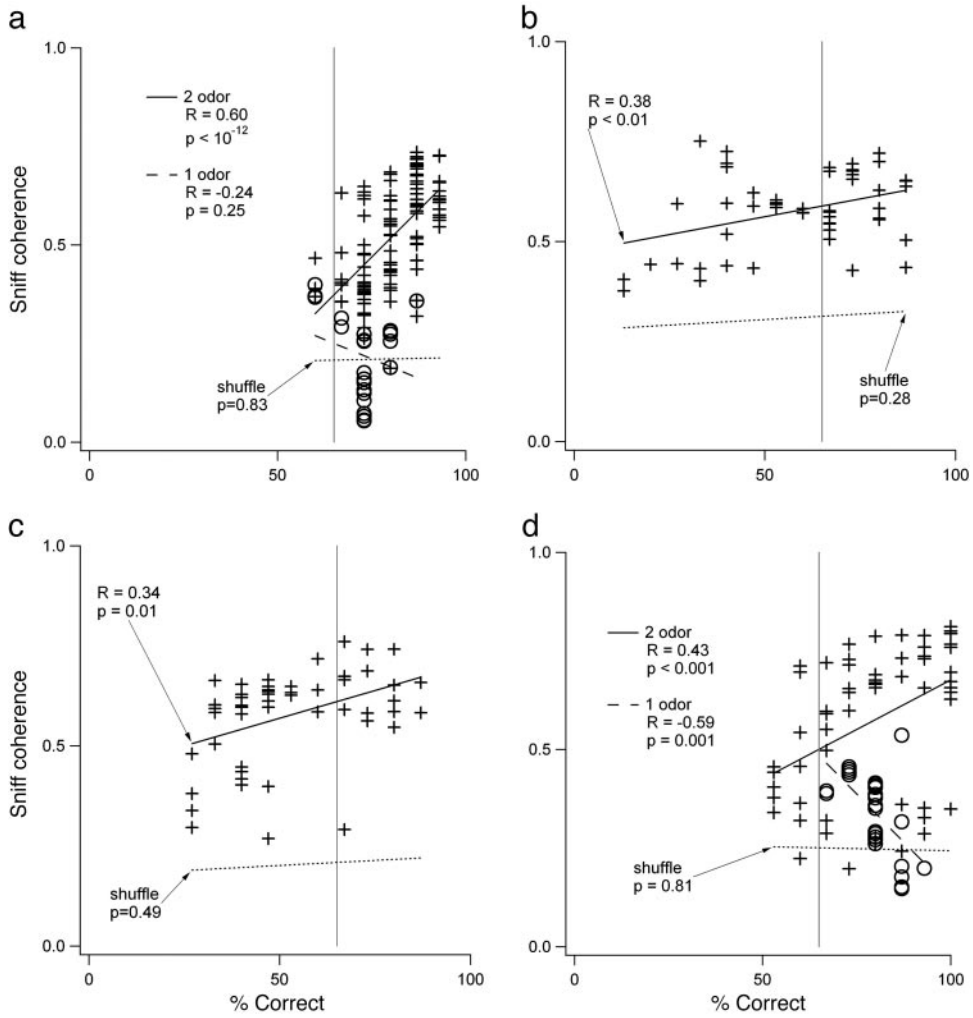

Fig. 5. Correlation between OB–HPC coherence and performance in the two-odor task is consistently positive. Coherence magnitude is the average coherence in the frequency band spanned by the peak OB and HPC high theta frequencies during odor sniffing. (*a*) Correlation plot for data from Fig. 4*c*. The crosses fit by the solid line show positive correlation in the two-odor condition (half-overlapping windows also show significant correlation; $R = 0.60$, $P < 0.05$). The open circles fit by the dashed line represent the CS^{+}-only run at the end of the session. Note that the correlation in this period is insignificant, even though some time windows do show significant coherence. The dashed line marked ''shuffle'' in all plots shows the correlation for the same data with the coherence estimated from OB and HPC data in mismatched trials. (*b*) Correlation for a different session from the same rat. (*c*) Correlation for a session from another rat (more examples in Fig. 10). (*d*) Positive correlation during the two-odor portion of a session and negative correlation during a one-odor run at the end. The longitudinal coherence plots for *b*, *c*, and *d* are in Fig. 11.

decreasing as performance increased, suggesting a negative correlation between coherence and performance. The results of that study indicate that the positive correlation reported here during performance of a well learned task may represent a process different from contingency learning.

Although correct trials are specifically defined by the behavior, incorrect trials could be of several types. Because of the relatively small number of false positive CS^{-} trials, the data cannot show whether OB–HPC coherence is predictive of a lever press to CS^{-}. However, OB–HPC coherence is present during correct CS^{-} trials without a lever press (Fig. 9), suggesting that this coherence is associated with the general task of odor discrimination, not the lever press itself. Because of the overlap between odor sampling and preparation for lever press in this study, these two processes cannot be completely distinguished. Ongoing studies in the laboratory address this issue by separating odor sampling from response periods.

The striking absence of EC–HPC coherence during odor sniffing suggests several interpretations: (*i*) HPC theta activity may drive theta activity in the OB, perhaps by means of the temporal pathway from CA1 nonpyramidal cells directly to the OB granule cell layer (25); (*ii*) during odor sniffing, the HPC is coherent with another part of the EC not recorded in this study; or (*iii*) the HPC does not directly influence the theta rhythm in the OB by means of a synaptic interaction, but they are both driven by the common respiratory process. The first alternative is supported by studies relating theta coherence over the extent of the HPC (26, 27) but would need validation by another method, such as selective temporal CA1 lesion. The second alternative suggests that different EC areas participate during resting theta and during fast sniffing. The EC electrodes in this study were positioned to span the cortical layers in the lateral EC, which receives OB input in rodents and projects to the HPC (CA1 and DG). The deep layers of the medial EC can be activated by repetitive lateral olfactory tract stimulation, which also evokes a large response in the DG and CA1, suggesting a feedback pathway from olfactory areas of the HPC to medial EC (28). In this case, HPC activity is presumed to drive the portion of the coherent OB theta signal by means of feedback through the medial EC. The third alternative is supported by reports that

the entire basal forebrain contains neurons that fire rhythmically with the respiratory cycle, particularly during periods of high respiratory drive (29, 30). Changes in hippocampal theta rhythm have also been correlated with respiratory state changes in rodents (31). Thus, it is likely that the HPC theta rhythm during the sniffing period is influenced by and influences respiratory processes and other theta-related brainstem–limbic system projections (32, 33). At the same time, afferent and centrifugal inputs drive a similar theta rhythm in the OB, producing a coherent signal by means of the common respiratory process. In this interpretation, sniffing becomes more than just respiration; it is also a major component of the cognitive effort in olfactory processing. More studies are needed to distinguish among these alternatives.

What functional role is played by OB–HPC theta band coherence? Theta power has been associated with sensorimotor processes (7), and one recent study has shown a dramatic decrease in theta power in the CA1 subfield associated with lever pressing for a reward (34). Figs. 2 and 3 together illustrate that, during periods of significant theta power decrease (odor sniffing in this case), there is, in fact, a significant rise in coherence between the OB and HPC at the sniff frequency. Thus, during periods of decreased power there may, in fact, be greater stimulus specificity within the HPC network represented by a sparser neural response.

Within-session longitudinal changes seen here are reminiscent of earlier studies, which showed dependence of HPC theta cell firing patterns and sensory-evoked potential amplitude on the pattern of a preceding short sequence of positive and/or negative reward trials (35, 36). It is possible that coherence magnitude is in some fashion related to the preceding trial sequence in the present study. However, it is equally possible that CS^+/CS^- structure (alternating trials versus runs in those studies) may simply modulate arousal and attention and, therefore, theta activity, similar to the change in the correlation sign shown here (Fig. 5 *a* and *d*).

These results are related to human studies showing theta-related performance statistics. In those studies, enhanced theta and alpha band coherence among various brain areas, including the HPC, were found to be correlated with high cognitive effort or performance (1–6). Increases in theta band power have also been associated with recall and peak performance on complex tasks (37, 38). From the data reported here, it is therefore proposed that sensory–hippocampal theta band coherence is a component in the neural mechanisms underlying cognitive effort and performance in sensorimotor tasks. In olfactory processing in particular, this coherence is associated with sniffing.

I thank Jennifer Beshel for helpful comments on the manuscript. L.M.K. was supported in part by a Brain Research Foundation Fay/Frank Seed Grant.

1. Razoumnikova, O. M. (2000) *Brain Res. Cognit. Brain Res.* **10,** 11–18.
2. Weiss, S., Muller, H. M. & Rappelsberger, P. (2000) *NeuroReport* **11,** 2357–2361.
3. Stowell, H. (1990) *Int. J. Neurosci.* **53,** 261–263.
4. Vernon, D., Egner, T., Cooper, N., Compton, T., Neilands, C., Sheri, A. & Gruzelier, J. (2003) *Int. J. Psychophysiol.* **47,** 75–85.
5. Raghavachari, S., Kahana, M. J., Rizzuto, D. S., Caplan, J. B., Kirschen, M. P., Bourgeois, B., Madsen, J. R. & Lisman, J. E. (2001) *J. Neurosci.* **21,** 3175–3183.
6. Sauseng, P., Klimesch, W., Doppelmayr, M., Hanslmayr, S., Schabus, M. & Gruber, W. R. (2004) *Neurosci. Lett.* **354,** 123–126.
7. Bland, B. H. & Oddie, S. D. (2001) *Behav. Brain Res.* **127,** 119–136.
8. Klingberg, F. & Pickenhain, L. (1965) *Acta Biol. Med. Ger.* **14,** 593–595.
9. Macrides, F. (1975) *Behav. Biol.* **14,** 295–308.
10. Ravel, N. & Pager, J. (1990) *Neurosci. Lett.* **115,** 213–218.
11. Kay, L. M. (2003) *J. Integr. Neurosci.* **2,** 31–44.
12. Kay, L. M. & Laurent, G. (1999) *Nat. Neurosci.* **2,** 1003–1009.
13. Hayar, A., Karnup, S., Shipley, M. T. & Ennis, M. (2004) *J. Neurosci.* **24,** 1190–1199.
14. Wiebe, S. P. & Staubli, U. V. (2001) *J. Neurosci.* **21,** 3955–3967.
15. Macrides, F., Eichenbaum, H. B. & Forbes, W. B. (1982) *J. Neurosci.* **2,** 1705–1717.
16. Vanderwolf, C. H. (1992) *Brain Res.* **593,** 197–208.
17. Kay, L. M. & Freeman, W. J. (1998) *Behav. Neurosci.* **112,** 541–553.
18. Kay, L. M., Lancaster, L. R. & Freeman, W. J. (1996) *Int. J. Neural Syst.* **7,** 489–495.
19. Bunsey, M. & Eichenbaum, H. (1993) *Behav. Neurosci.* **107,** 740–747.
20. Truchet, B., Chaillan, F. A., Soumireu-Mourat, B. & Roman, F. S. (2002) *Hippocampus* **12,** 600–608.
21. Alvarez, P., Wendelken, L. & Eichenbaum, H. (2002) *Neurobiol. Learn Mem.* **78,** 470–476.
22. Hess, U. S., Lynch, G. & Gall, C. M. (1995) *J. Neurosci.* **15,** 7796–7809.
23. Dusek, J. A. & Eichenbaum, H. (1997) *Proc. Natl. Acad. Sci. USA* **94,** 7109–7114.
24. Wirth, S., Ferry, B. & Di Scala, G. (1998) *Behav. Brain Res.* **91,** 49–59.
25. van Groen, T. & Wyss, J. M. (1990) *J. Comp. Neurol.* **302,** 515–528.
26. Buzsaki, G., Chen, L. S. & Gage, F. H. (1990) *Prog. Brain Res.* **83,** 257–268.
27. Buzsaki, G. (2002) *Neuron* **33,** 325–340.
28. Biella, G. & de Curtis, M. (2000) *J. Neurophysiol.* **83,** 1924–1931.
29. Manns, I. D., Alonso, A. & Jones, B. E. (2003) *J. Neurophysiol.* **89,** 1057–1066.
30. Chen, Z., Eldridge, F. & Wagner, P. (1991) *J. Physiol. (London)* **437,** 305–325.
31. Harper, R. M., Poe, G. R., Rector, D. M. & Kristensen, M. P. (1998) *Neurosci. Biobehav. Rev.* **22,** 233–236.
32. Kocsis, B., Di Prisco, G. V. & Vertes, R. P. (2001) *Eur. J. Neurosci.* **13,** 381–388.
33. Olucha-Bordonau, F. E., Teruel, V., Barcia-Gonzalez, J., Ruiz-Torner, A., Valverde-Navarro, A. A. & Martinez-Soriano, F. (2003) *J. Comp. Neurol.* **464,** 62–97.
34. Wyble, B. P., Hyman, J. M., Rossi, C. A. & Hasselmo, M. E. (2004) *Hippocampus* **14,** 662–674.
35. Deadwyler, S. A., West, M. O., Christian, E. P., Hampson, R. E. & Foster, T. C. (1985) *Behav. Neural Biol.* **44,** 201–212.
36. Foster, T. C., Christian, E. P., Hampson, R. E., Campbell, K. A. & Deadwyler, S. A. (1987) *Brain Res.* **408,** 86–96.
37. Kahana, M. J., Sekuler, R., Caplan, J. B., Kirschen, M. & Madsen, J. R. (1999) *Nature* **399,** 781–784.
38. Egner, T. & Gruzelier, J. H. (2003) *NeuroReport* **14,** 1221–1224.